V_6O_{13} AS CATHODE MATERIAL FOR LITHIUM CELLS*

K. WEST, B. ZACHAU-CHRISTIANSEN, T. JACOBSEN and S. ATLUNG

Fysisk-Kemisk Institut, The Technical University of Denmark, DK 2800 Lyngby (Denmark)

Summary

The e.m.f. *vs.* composition relationship of $Li/Li_xV_6O_{13}$ has been studied at 25 °C and 155 °C by cyclic voltammetry using organic and polymeric electrolytes, respectively. At both temperatures the lithium insertion reaction is found to be reversible in the composition interval: $0 \leqslant x \leqslant 8$. a.c.-impedance measurements on single crystals (25 °C) show that Li^+ diffusion in $Li_xV_6O_{13}$ is one dimensional and proceeds along the channels in the *b* axis direction. Cycling of $Li/Li_xV_6O_{13}$ cells with organic and polymer electrolyte shows that high materials utilization and good cycling performance can be achieved with both systems. It is demonstrated that $Li_xV_6O_{13}$ is sensitive to discharge below 1 V *vs.* Li.

Introduction

The use of V_6O_{13} as active material for positive electrodes in secondary lithium batteries was first suggested in 1979 by Murphy and coworkers [1, 2]. Since then Li/V_6O_{13} has been studied by several groups [3 - 13], and important differences in properties between this material and the much studied titanium disulphide (TiS_2) have been discovered.

For battery applications, the property most in favour of V_6O_{13} is the high stoichiometric energy density. 890 W h/kg is determined for the ultimate composition $Li_8V_6O_{13}$ [13], and this is considerably greater than the 490 W h/kg achieved for $LiTiS_2$ [14]. There is, however, some dispute regarding the number of Li ions that can be reversibly cycled in $Li_xV_6O_{13}$ electrodes [4, 5, 9, 10, 13].

As highly lithiated V_6O_{13} is a poor electronic conductor [13], the practical energy density will be reduced by the necessity for the addition of electronically conductive material, *e.g.*, graphite or acetylene black.

Structurally, V_6O_{13} and TiS_2 belong to different classes: TiS_2 is a layered, two-dimensional conductor in which the lithium ions are distributed over a number of equivalent, octahedrally coordinated sites. The smoothly

*Based on a paper presented at the 2nd International Meeting on Lithium Batteries, Paris, April 25 - 27, 1984.

0378-7753/85/$3.30

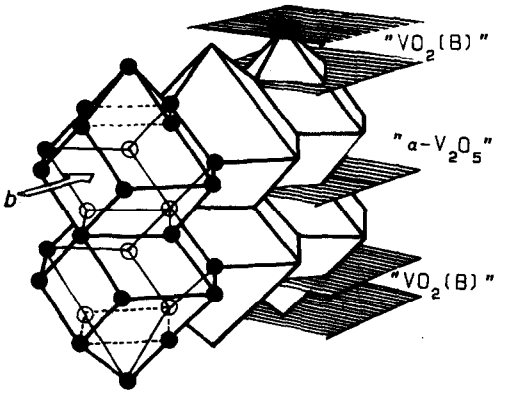

Fig. 1. Chain of double cavities in V_6O_{13}. Only the oxygen atoms indicating the cavity and the planes of the vanadium atoms are shown. The structure can be visualised as a stack of VO_2(B)- and α-V_2O_5-sheets joined at octahedra corners.

sloping e.m.f. curve of Li/Li_xTiS_2 can be quantitatively explained by a simple lattice gas model based on the electrostatic interaction between the inserted lithium ions [15]. In V_6O_{13}, however, Li^+ conduction is virtually one-dimensional, with lithium ions residing in double channels of interconnected, perovskite-like cavities, as shown in Fig. 1. As there are a number of different sites in these cavities, the e.m.f. curve of $Li/Li_xV_6O_{13}$ shows several distinct plateaus, reflecting the sequential filling of inequivalent sites. The interaction between the inserted ions and the host lattice is also expressed in a rather high (15%) expansion of the unit cell volume upon lithium insertion [8, 13].

In this paper thermodynamic and transport properties, as well as cycling results, are reported for $Li/Li_xV_6O_{13}$ cells with organic electrolyte operating at 25 °C and with polymeric electrolyte operating at 155 °C. So far no single electrolyte covering this temperature interval is known.

Experimental

V_6O_{13} powders were prepared and analysed as previously described [13]. The stoichiometry of the material used in these investigations was $V_6O_{12.86}$, determined by chemical analysis. Stoichiometric single crystals were grown from this powder and the proper amount of V_2O_5 in evacuated quartz ampoules, using $TeCl_4$ as transporting agent.

Measurements at 25 °C were carried out using 1M $LiAsF_6$ (USS Agri Chemicals) solutions in distilled propylene carbonate (PC) as electrolyte, either in three-electrode test cells [14] or in hermetically sealed button cells with pressed pellet electrodes consisting of 75 wt.% $V_6O_{12.86}$, 20 wt.% acetylene black (Shawinigan, 50% compressed) and 5 wt.% PTFE. These pellets were pressed into expanded nickel grids (100 - 140 °C, 400 MPa) to improve mechanical stability and electronic conductance.

Measurements at 155 °C were carried out using thin layer cells, consisting of a lithium foil and a composite electrode film with overall composition: 65 wt.% $V_6O_{12.86}$; 7 wt.% acetylene black; 6 wt.% $LiCF_3SO_3$ (3M "FC 124", recrystallized from acetonitrile), and 22 wt.% poly(ethylene oxide) (BDH "Polyox WSR 301"). This formulation was chosen to give an approximate electrolyte volume of 50% which is also the estimated porosity of the pressed pellet electrodes. The separator was 1 or 2 layers of 50 μm $LiCF_3SO_3$/PEO film with a lithium to oxygen ratio $\approx$ 1:14.

The composite electrode films were cast on nickel foil from a dispersion/solution of all the electrode compounds in acetonitrile ($\approx$ 8 wt.%). It has proven to be of utmost importance for cell performance that this dispersion is uniform, ensuring a low void volume of the resulting film. The cell assembly was spring loaded and heated in a Buchi TO-50 oven slightly pressurized with argon.

The amount of active material was determined by chemical analysis of exhausted cells.

The a.c. impedance of different single crystal surfaces (identified by X-ray diffraction) in contact with $LiAsF_6$/PC electrolyte was determined in the frequency range 16 kHz - 0.4 mHz using an automated frequency response analyzer (Solartron 1174).

Results and discussion

E.m.f. curve

Lithium insertion into V_6O_{13} was studied by cyclic voltammetry, and a voltammogram obtained at 25 °C (sweep rate: 10 μV/s) is shown in Fig. 2. It is seen that insertion occurs essentially in three potential regions,

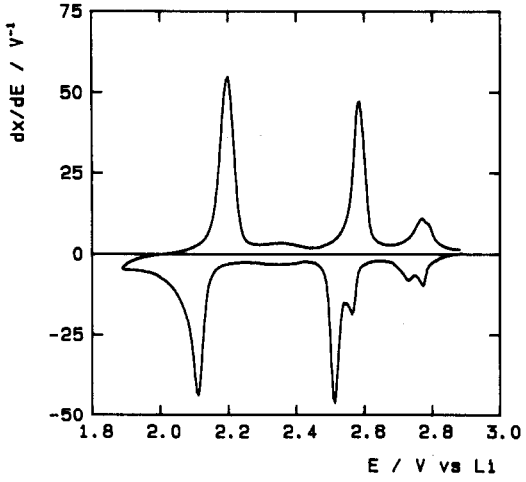

Fig. 2. Voltammogram of $Li/Li_xV_6O_{13}$ in $LiAsF_6$/PC, 25 °C. The current is normalized as dx/dE, assuming that the composition at 2.2 V *vs.* Li is $Li_4V_6O_{13}$. Sweep rate = 10 μV/s.

corresponding to the three main plateaus of the e.m.f. curve [13]. The set of peaks around 2.15 V *vs.* Li is characteristic of a two-phase region, showing no overlap between the anodic and the cathodic peak, but with their front edges on a straight line intersecting zero current at the two-phase potential. This separation of the peaks arises because changes in composition can occur only when the two-phase potential is exceeded. The shape of the peaks at 2.55 and 2.75 V is more complex, with partial overlap and splitting of the cathodic peaks. The lithium insertion in these regions is believed to proceed either as single-phase reactions or as two-phase reactions with narrow miscibility gaps and broad homogeneity ranges of the involved phases.

Counting the charges in each peak region, it can be seen that they correspond to the insertion of 1 (2.75 V), 3 (2.55 V), and 4 (2.15 V) Li per formula unit. In the cavities shown in Fig. 1, the highest oxygen to lithium coordination, 5, is obtained when lithium occupies the square pyramidal sites formed by the apexes of the cavities. As the two cavities per formula unit contain only 6 of these sites, other types of sites capable of accommodating lithium must be present in the structure. As coordination to oxygen is a critical factor in stabilization of inserted lithium, these sites are most likely to be the square faces joining the cavities, with the possibility of coordination to 4 coplanar oxygens. This leads to a total of 9 possible sites per formula unit. In a previous paper it was argued that the amount of lithium inserted into V_6O_{13} was limited not by the number of lithium sites but by the number of electronic sites available [13].

As the insertion of 1 Li/6V (*i.e.*, 2 Li per unit cell) corresponds to a completed structure, it is likely that the initial insertion occupies a special (two-fold) position, not breaking the original symmetry. The square planar sites in the "V_2O_5"-layer have this multiplicity, and in this layer repulsion from V atoms is less than in the more V containing "VO_2(B)" layers. Further lithium insertion leads to occupation of the square pyramidal sites between the "V_2O_5" and the "VO_2(B)" layers, displacing the first Li atoms to these sites and giving a filled structure with 4 Li/6V of high symmetry. In the last stage, the 4 remaining lithium ions enter the pyramidal site in the VO_2(B) planes and the four coordinated sites connecting the cavities.

Voltammograms obtained with a (V_6O_{13}/acetylene black/polymeric electrolyte)-composite electrode at 155 °C are shown in Fig. 3 (sweep rate: 10 μV/s). It is seen that the peaks at 2.75 V and 2.55 V in the room temperature voltammogram split into 4 separate peaks in the cathodic scan of the high temperature voltammogram (peak potentials: 2.86 V, 2.75 V, 2.59 V, and 2.43 V). Also, the set of peaks at 2.15 V shows a splitting of the anodic peak, but the two-phase potential has not changed. On repeated cycling, the electrode capacity decreases drastically, but the qualitative features of the voltammogram are unchanged except for the vanishing of the small cathodic peak at 2.86 V. Hence, the capacity decrease can be ascribed to loss of contact between electrode components, leaving the lithium insertion process basically reversible at 155 °C, as it is at 25 °C.

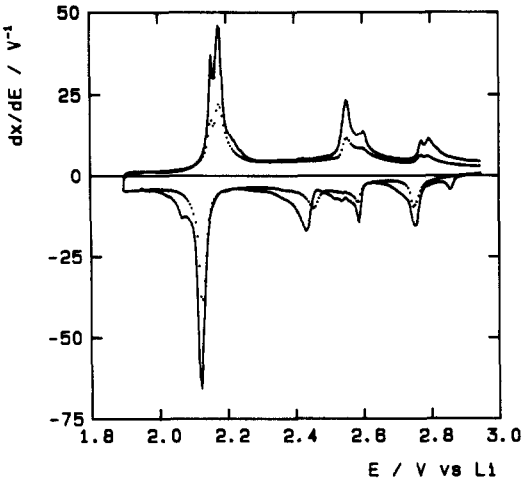

Fig. 3. Voltammogram of $Li/Li_xV_6O_{13}$ in $LiCF_3SO_3/PEO$, 155 °C. ——: first sweep; ·····: second sweep. The current is normalized as dx/dE, assuming that the composition at 2.2 V *vs.* Li is $Li_4V_6O_{13}$ in the first sweep. Sweep rate = 10 μV/s.

The constant current discharge curves at 25 °C and 155 °C (Figs. 8 and 10) show plateaux corresponding to all the peaks in the voltammograms.

Transport properties

Measured a.c. impedances at 2.600 V *vs.* Li (25 °C, $LiAsF_6$/PC electrolyte) are shown in Fig. 4. For the polished (0, 1, 0) surface a suppressed semicircle followed by a straight line with a slope close to unity at low frequencies is observed. This behaviour can be explained by an adsorption of Li^+ ions followed by a desolvating transfer reaction and subsequent diffusion of Li^+ ions into the solid phase. The transfer resistance of 90 Ω cm^2 and double layer capacity of 27 μF cm^{-2}, calculated from the semicircle, appear as reasonable values. In the case of the naturally grown and rather imperfect (1, 0, 1) surface, the semicircle is also obtained, but the low frequency range indicates limited transfer into the bulk material. Finally, for the very smooth (0, 0, 1) surface, the semicircle is not observed and the low frequency impedances are two orders of magnitude higher than those found for the (0, 1, 0) surface. The limited solid state diffusion found at the (0, 0, 1) and (1, 0, 1) surfaces can be explained as being due to (0, 1, 0) surfaces exposed at imperfections such as kinks. It is concluded that Li^+ diffusion in $Li_xV_6O_{13}$ is one dimensional and proceeds along the channels in the *b* axis direction.

At potentials below 2.5 V the high frequency semicircle is gradually deformed. At low potentials, extremely low and almost constant phase angles are obtained as shown in Fig. 5. At present, no satisfactory explanation for these phase angles being as low as 10° has been found. As the low phase angle is still present after subsequent equilibration of the crystal at

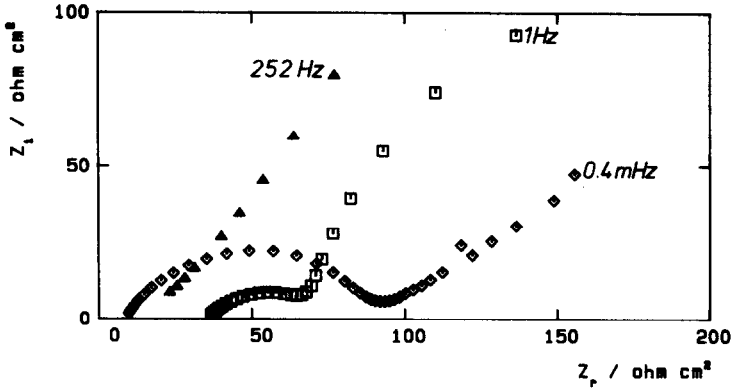

Fig. 4. Complex impedance of V_6O_{13} single crystal, E = 2.600 V. Surfaces exposed: ◇, (0, 1, 0) polished; □, (1, 0, 1) natural (30 ohm added); △, (0, 0, 1) natural. Minimum frequencies indicated.

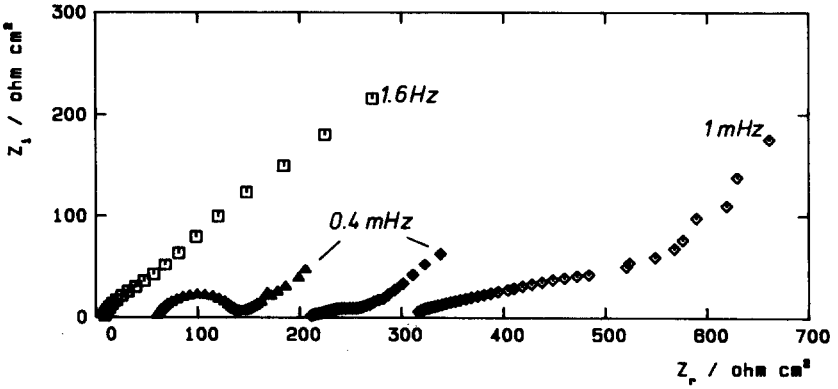

Fig. 5. Complex impedance of V_6O_{13} single crystal. Electrode potential *vs.* Li: □, 3.000 V; △, 2.600 V (50 ohm added); ♦, 2.300 V (200 ohm added); ◇, 2.100 V (300 ohm added). Minimum frequencies indicated.

potentials above 2.5 V, a partial explanation may be the formation of cracks in the surface caused by lattice expansions during insertion.

The lithium ion diffusion coefficient, $\tilde{D}_{Li}$, can, in principle, be calculated from the $(j\omega)^{-1/2}$ component of the low frequency impedance according to the equation:

$$\tilde{D}_{Li} = \left(- \frac{dE/dx}{Fc_1 Z_d (j\omega)^{1/2}} \right) \quad (1)$$

where dE/dx is the slope of the e.m.f. *vs.* composition (x) relation, c_1 is the volume concentration of Li inserted for $x = 1$ and Z_d is the low frequency impedance. However, in two-phase regions dE/dx is zero and eqn. (1) is not valid. dE/dx can be determined either directly from an infinitely

slow voltammogram, *i.e.*, a voltammogram with no hysteresis between the anodic and the cathodic scan, or from numerical differentiation of the e.m.f. *vs.* x relationship. The voltammogram shown in Fig. 2 shows a pronounced hysteresis around the peaks, and the e.m.f. curve determined from equilibrated samples [13] has not yet been established with an accuracy allowing numerical differentiation. Between the peaks however, the cyclic voltammogram shows reversible regions, and using dE/dx values determined here the values in Table 1 for $\tilde{D}_{Li}$ have been calculated from eqn. (1).

TABLE 1

Lithium ion diffusion coefficients (25 °C) determined from a.c. impedances

E (V)	$\tilde{D}_{Li}$ ($cm^2\ s^{-1}$)	x
2.800	3×10^{-9}	0.27
2.600	9×10^{-9}	1.3
2.300	3×10^{-9}	3.9

From galvanostatic pulse measurements on powders $\tilde{D}_{Li}$ values of 2×10^{-8} ($x = 0.7$) and 8×10^{-9} $cm^2\ s^{-1}$ ($x = 2.5$) have previously been reported [6, 11]. Taking into account the uncertainty in the determination of dE/dx common to all linear methods based on semi-infinite diffusion, these values are in accordance with those of the present work. Considerably lower values decreasing from 8×10^{-10} ($x = 0.5$) to 6×10^{-11} $cm^2\ s^{-1}$ ($x = 6$) with increasing insertion have been found in the potential regions around the peaks in the voltammograms by a non-linear technique based on time constants [13]. As the main part of the available capacity is in these potential regions, the latter values, which include any kinetic factors from phase transformations as well, should be used for design of electrodes.

Cycling experiments

In order to investigate the long term reversibility of the lithium insertion reaction in V_6O_{13}, button cells with $LiAsF_6$/PC electrolyte, and thin film cells with $LiCF_3SO_3$/PEO electrolyte were cycled at room temperature and 155 °C, respectively. To avoid problems with overcharge and overdischarge, the cycling procedure chosen was galvanostatic discharge to 1.80 V, corresponding to insertion of 8 Li per formula unit in the surface of the contacted electrode material, followed by current limited potentiostatic recharge to 2.90 V.

Figure 6 shows a plot of electrode utilization *vs.* cycle number for a button cell with a 290 μm V_6O_{13}/C/PTFE pellet. The utilization is calculated on the basis of all the V_6O_{13} present in the cell. The cell was discharged with 1 mA/cm^2, corresponding to a stoichiometric discharge time of 7.7 h (8 Li/V_6O_{13}). The average materials utilization during the first 100 cycles was ≈ 4.3 e^-/V_6O_{13}. In liquid organic electrolyte, poor cycling

efficiency of the lithium electrode often has a great influence on the available cell capacity, and the steady capacity loss on cycling shown in Fig. 6 is both due to cathodic deterioration and to the build up of a thick, spongy layer of uncontacted lithium grains on the lithium electrode.

Using small amounts of electrolyte carefully dried with Al_2O_3, cleaning all construction parts of the cell by refluxing in methanol, and securing a steady pressure on the cell stack, it is possible to reduce this problem, and a constant, high electrode utilization can be achieved as shown in Fig. 7 (stoichiometric discharge time: 8.2 h). The integrity of the cathode material is evidenced by the unchanged shape of the discharge curve during cycling, exhibiting all the plateaux of the e.m.f. curve (Fig. 8). In cycle #31, the cell was discharged to 0.4 V. From Fig. 8 it is seen that the cell has a substantial capacity below 1 V, but it is also evident from the subsequent cycles that discharging the cell to this low potential had caused irreversible loss of cell capacity. *Post mortem* analysis of this cell showed the lithium electrode to be covered with a brown, pasty layer, quite different in appearance from the layer of uncontacted lithium grains often seen in these cells.

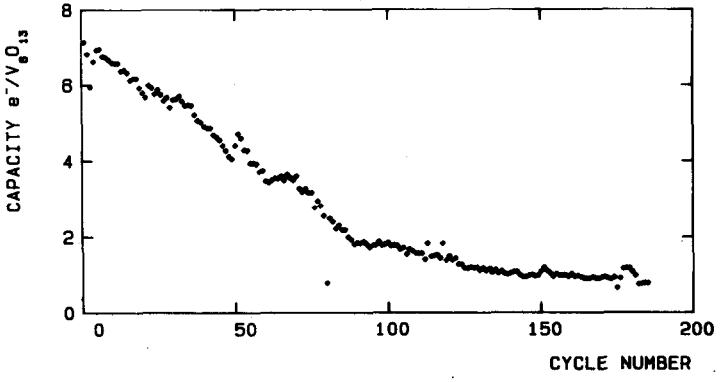

Fig. 6. Cathode utilization (number of inserted lithium ions per formula unit) *vs.* cycle number for Li/V_6O_{13} cells with $LiAsF_6$/PC electrolyte, 25 °C. Discharge current density = 1 mA/cm^2.

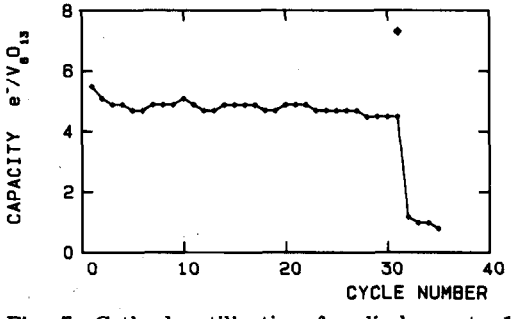

Fig. 7. Cathode utilization for discharge to 1.8 V *vs.* cycle number for improved Li/V_6O_{13} cells with $LiAsF_6$/PC electrolyte, 25 °C. Discharge current density = 0.75 mA/cm^2. ♦: discharge capacity to 0.4 V.

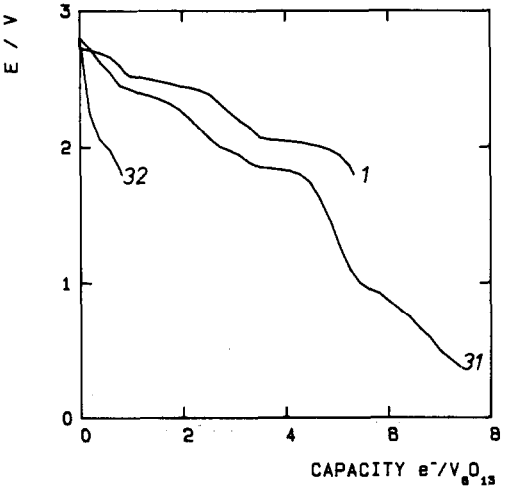

Fig. 8. Discharge curves #1, #31, and #32 of the cell shown in Fig. 7.

Cycling of lithium in contact with $LiCF_3SO_3$/PEO electrolyte (155 °C) apparently proceeds with high cycling efficiency, as no sign of degradation of the lithium electrode is seen after prolonged cycling. In the cycling experiment shown in Fig. 9, a 50 μm V_6O_{13}/C/PEO/$LiCF_3SO_3$ film electrode was discharged with 0.44 mA/cm^2, corresponding to a stoichiometric discharge time of 5.8 h. During cycles #24 to #29 a temporary failure in the test system caused incomplete recharge of the cell. The total amount of lithium plated during the life of this cell corresponds to a 750 μm thick layer. *Post mortem* analysis of the cell showed the bulk of the 250 μm lithium electrode to consist of shiny lithium metal. As the separator electrolyte sticks to the lithium surface, the lithium/electrolyte interface could not be inspected directly.

In the first discharge, the capacity of the cell was 7.2 e^-/V_6O_{13}. In the next cycles the cell capacity decreases rapidly, but after cycle #10 only small amounts of capacity are lost in each cycle. The average materials utilization during the first 100 cycles was ≈ 3.6 e^-/V_6O_{13}. The charging efficiency, defined as the ratio between charge output and charge input to the cell during one complete cycle, is close to unity up to cycle #100. In the last cycles, the capacity decrease is accompanied by a decrease in charging efficiency. This indicates that the failure mode is "soft dendrites" [16], *i.e.*, increased charge input due to intermittent dendrite bridging.

Three representative discharge curves are shown in Fig. 10. Apparently, the initial capacity decrease in this case is due to loss of the 2.15 V plateau. This is, however, not generally the case for these cells, as other cells with the same composition, but with a higher stack pressure, retain all the plateaux on the discharge curve during cycling, without improvements in overall cell performance, however. It is believed that the principal cause of capacity decrease is loss of contact between electrode components,

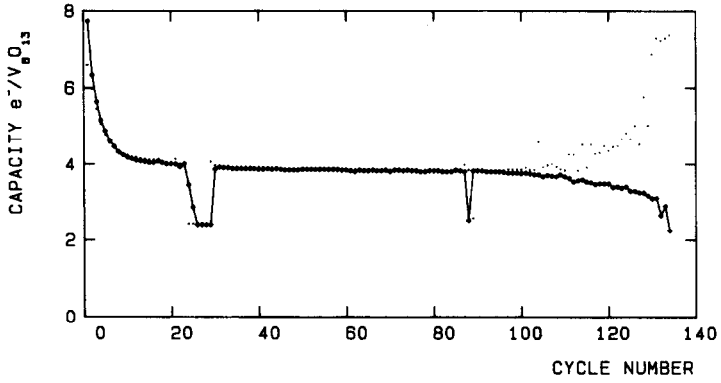

Fig. 9. Cathode utilization *vs.* cycle number for Li/V_6O_{13} cells with $LiCF_3SO_3$/PEO electrolyte, 155 °C. Discharge current density = 0.44 mA/cm^2. Recharge capacity shown as dots.

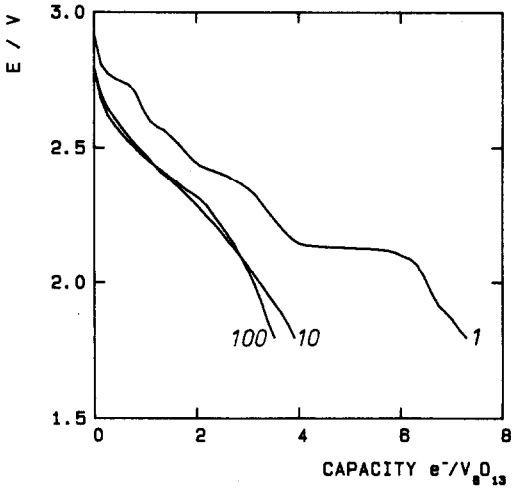

Fig. 10. Discharge curves #1, #10, and #100 of the cell shown in Fig. 9.

especially to lithium saturated V_6O_{13}, which is a very poor electronic conductor. The cause of this electrode deterioration is probably the large volume change of V_6O_{13} upon lithium insertion.

Conclusion

Insertion of lithium in V_6O_{13} is basically a reversible process at 155 °C as well as at room temperature, with a very high stoichiometric energy density (890 W h/kg at 25 °C).

Cycling of $Li/Li_xV_6O_{13}$ cells with liquid organic electrolyte (room temperature), and with quasi-solid polymer electrolyte (155 °C) shows that

high materials utilization and good cycling performance can be achieved in both systems as long as overdischarge is avoided.

Whereas the primary failure mode of the cells with liquid organic electrolyte was the poor cycling efficiency of the lithium electrode, lithium apparently cycles well in contact with polymer electrolyte.

The high stoichiometric energy density of the $Li/Li_xV_6O_{13}$ couple compared with other insertion materials (*e.g.*, Li_xTiS_2) is, to some extent, offset by the required addition of conductive material to practical V_6O_{13}-based electrodes, and by the capacity losses on cycling of these electrodes.

The most severe capacity decrease is observed in the initial cycles of the cells with polymer electrolyte, but in view of the inherent reversibility of the lithium insertion process, it is believed that improvements in electrode fabrication techniques will lead to longer cycle lives of these cells.

Acknowledgements

This work was supported by the Danish Department of Energy and by the EEC. Helpful discussions with colleagues in the Joint Danish–British Energy Research Programme are greatly acknowledged.

References

1 D. W. Murphy, P. A. Christian, F. J. DiSalvo and J. N. Carides, *J. Electrochem. Soc., 126* (1979) 497.
2 D. W. Murphy and P. A. Christian, *Science, 205* (1979) 651.
3 D. W. Murphy, P. A. Christian, F. J. DiSalvo, J. N. Carides and J. V. Waszcak, *J. Electrochem. Soc., 128* (1981) 2053.
4 K. M. Abraham, J. L. Goldman, M. D. Dempsey and G. L. Holleck, Exploratory development of an electrically rechargeable lithium battery, *AD A093038, Oct. 1980.*
5 K. M. Abraham, J. L. Goldman and M. D. Dempsey, *J. Electrochem. Soc., 128* (1981) 2493.
6 P. C. Spurdens, J. Drennan, J. R. Owen, B. C. H. Steele, J. M. Gonzales-Calbert and D. A. Jefferson, *Solid State Ionics, 5* (1981) 335.
7 J. R. Owen, J. Drennan, G. E. Lagos, P. C. Spurdens and B. C. H. Steele, *Solid State Ionics, 5* (1981) 343.
8 B. C. H. Steele, G. E. Lagos, P. C. Spurdens, C. Forsyth and A. D. Foord, *Solid State Ionics, 9 and 10* (1983) 391.
9 E. J. Frazer and S. Phang, *J. Power Sources, 10* (1983) 33.
10 S-N. Hua and S. Phang, *J. Power Sources, 10* (1983) 279.
11 P. G. Dickens and G. J. Reynolds, *Solid State Ionics, 5* (1981) 331.
12 A. Hooper and J. North, *Solid State Ionics, 9 and 10* (1983) 1161.
13 K. West, B. Zachau-Christiansen and T. Jacobsen, *Electrochim. Acta, 28* (1983) 1829.
14 K. West, T. Jacobsen, B. Zachau-Christiansen and S. Atlung, *Electrochim. Acta, 28* (1983) 97.
15 T. Jacobsen, K. West and S. Atlung, *Electrochim. Acta, 27* (1982) 1007.
16 G. L. Holleck, K. M. Abraham, P. B. Harris, J. L. Goldman, J. Avery, M. W. Rupich and S. B. Brummer, *Proc. 30th Power Sources Symp.*, 1982, p. 68.